PFC/JA-90-20

Propagation and Damping of Mode Converted Ion-Bernstein Waves in Toroidal Plasmas

A. K. Ram and A. Bers

June 1990

Plasma Fusion Center
Massachusetts Institute of Technology
Cambridge, MA 02139 USA

Submitted for Publication in *The Physics of Fluids B*

Propagation and Damping of Mode Converted

Ion-Bernstein Waves in Toroidal Plasmas

A. K. Ram and A. Bers

TABLE OF CONTENTS

PROPAGATION AND DAMPING OF MODE CONVERTED ION-BERNSTEIN WAVES IN TOROIDAL PLASMAS

A. K. Ram and A. Bers

Plasma Fusion Center and Research Laboratory of Electronics

Massachusetts Institute of Technology

Cambridge, MA 02139

ABSTRACT

In the heating of tokamak plasmas by waves in the ion-cyclotron range of frequencies the fast Alfvén waves launched at the plasma edge can mode convert to the ion-Bernstein waves (IBW). We study the propagation and damping of these mode converted waves using a ray tracing code which follows the fast phase and the amplitude of the electromagnetic field along the IBW ray trajectories in a toroidal plasma. A simple analytical model is developed which describes the numerically observed features of propagation and damping of the IBW's. We find that along the ray trajectory of the IBW there is an upshift of the poloidal mode numbers which can lead to the electron Landau damping of the wave. This damping is dependent on the strength of the toroidal plasma current. From the properties of the upshift of the poloidal mode numbers we conclude that the mode converted ion-Bernstein waves are not suitable candidates for electron current drive.

PACS numbers: 52.50.Gj, 52.40.Db

I. INTRODUCTION

The heating of tokamak plasmas by radio-frequency waves in the ion-cyclotron range of frequencies (ICRF) has been of extensive experimental and theoretical interest in recent years.[1,2,3] ICRF heating has been demonstrated successfully on a variety of tokamaks which, as a consequence, has led to an increased theoretical interest. During ICRF heating the fast Alfvén wave (FAW) is excited at the edge of the plasma and then propagates towards the center of the plasma. In a plasma with two (a majority and a minority) ion species, the FAW propagates on either side of the ion-ion hybrid resonance. For small $k_{\|}$ (the wave number parallel to the total magnetic field), a FAW launched from a region of low magnetic field can couple to an ion-Bernstein wave (IBW) towards the high-field side of the ion-ion hybrid resonance.[4] However, fast Alfvén waves incident from the high magnetic field region undergo mode conversion directly to the IBW's.[4] While the propagation and damping of the FAW at the cyclotron resonance and at the ion-ion hybrid resonance have been extensively studied, little is known about the propagation and damping of the IBW that is generated by mode conversion of the FAW. In this paper we study the propagation characteristics of these mode converted IBW's in a toroidal plasma. Towards this end we have developed a numerical ray tracing code for following the IBW's in toroidal plasmas.[5,6] In this code the full dielectric tensor for a hot, Maxwellian plasma[7] is used in a toroidal geometry. The equilibrium configuration is prescribed and the code follows the amplitude and the phase of the rays. The amplitude equation includes the effects of focusing[8] and is similar to a code developed earlier.[9] Although we use our code to study the IBW it can be used to study the propagation of waves of any frequency.

The numerical results for the IBW ray trajectories are used to construct a simple analytical model that gives general guidelines about the propagation and damping of IBW's in toroidal plasmas. Although the model is constructed by making simplifying assumptions which restrict its domain of validity, nevertheless, we can make qualitative and quantitative predictions which are verified numerically. The important features that follow from the analysis are that the IBW's primarily impart their energy to electrons as the magnitude of the poloidal mode numbers upshifts during their toroidal propagation, and that the spatial location of this electron Landau damping is dependent on the magnitude of the plasma

current. Furthermore, we find that the IBW's are not suitable for electron current drive. Electrons with positive parallel (to the total magnetic field) phase velocities damp the IBW's below the equatorial plane of the tokamak, while electrons with negative parallel phase velocities damp the IBW's above the equatorial plane.

In trying to solve the complete problem of ICRF heating it would be necessary to know the fraction of the total FAW power that is converted to the IBW. This is the problem addressed by mode conversion theories.[4,10] In this paper we do not attempt to solve this problem. We are primarily concerned with the propagation properties of the IBW and their dependence on plasma parameters. Furthermore, by starting the IBW ray propagation after the mode conversion region we avoid all regions of resonances (cyclotron harmonic, ion-ion-hybrid) and cut-offs (edge region of the plasma, mode conversion region) where the geometrical optics approximations are certainly not valid.

The paper is organized as follows. In Section II we outline the equations used for following the trajectories and amplitudes of the IBW rays. In Section III we describe numerical results, obtained from the computer code, which are subsequently used in Section IV to develop a general analytical picture of the properties of IBW propagation in toroidal plasmas. In Section V we discuss the effects of including the focusing term in the equation for the evolution of the electric field amplitude. The essential conclusions from our numerical and analytical analysis are outlined in Section VI.

II. RAY TRAJECTORY AND AMPLITUDE EVOLUTION EQUATIONS

The geometrical optics equations describing the propagation of rays through a spatially varying, weakly dissipative plasmas are:[8,11]

$$\frac{d\vec{k}}{dt} = \frac{(\partial D/\partial \vec{r})}{(\partial D/\partial \omega)}, \qquad \frac{d\vec{r}}{dt} = -\frac{(\partial D/\partial \vec{k})}{(\partial D/\partial \omega)} \tag{1}$$

where $D = D(\vec{k},\omega,\vec{r}) = det(\overline{\overline{D}}^{H})$, $\overline{\overline{D}}^{H}$ is the hermitian part of the dispersion tensor, $\overline{\overline{D}}$, describing the plasma, $\vec{r}$ is the position vector, $\vec{k}$ is the wave vector and ω is the frequency. The electric field along the ray is assumed to be of the form $\vec{E}(\vec{r},t) = Re\Big\{\vec{E}_0(\vec{r})\ exp[i\psi(\vec{r},t)]\Big\}$ where $\vec{E}_0$ is assumed to be the slowly varying amplitude, $\vec{k}(\vec{r}) = \nabla\psi$, and $\omega(\vec{r}) = -\partial\psi/\partial t$. The magnetic field of the ray is then determined through

Maxwell's equations. The t with respect to which the derivatives in (1) are evaluated is the time along the ray trajectory. Thus, $|\vec{v}_g|t$, where $\vec{v}_g$ is the group velocity of the ray, gives the spatial distance travelled by the ray in time t. The equations in (1) are Hamiltonian in structure with $\omega = \omega(\vec{k}(\vec{r}), \vec{r})$ (obtained by solving $D = 0$) being the Hamiltonian.[12,13,14] This is useful since one can perform point transformations from the Cartesian coordinate system to some other orthogonal coordinate system without changing the form of the ray trajectory equations (1). In particular, this is true for the toroidal coordinate system which we will be using. In this system we define $\vec{r} = (r, \theta, \phi)$ where r is the radius measured from the magnetic axis of the torus, θ is the poloidal angle, and ϕ is the toroidal angle; $\vec{k} = (k_r, m, n)$ where k_r, m and n are the radial, poloidal and toroidal components, respectively, of the wave vector. A relation that will be useful in our later analyses is that connecting the toroidal wave vector components to the Cartesian components:

$$k_{\|} = k_r B_r + \left(\frac{m}{r}\right)\frac{B_\theta}{B} + \left(\frac{n}{R + r cos\theta}\right)\frac{B_\phi}{B} \tag{2}$$

$$k_\perp^2 = k_r^2 + \left(\frac{m}{r}\right)^2 + \left(\frac{n}{R + r cos\theta}\right)^2 - {k_{\|}}^2 \tag{3}$$

where $\vec{B} = (B_r, B_\theta, B_\phi)$ is the magnetic field in toroidal coordinates, $B = |\vec{B}|$, R is the major radius of the tokamak, and $k_{\|}$ and $k_\perp$ are the components of $\vec{k}$ that are parallel and perpendicular to $\vec{B}$, respectively. The spatial variations in the density, temperature, and the magnetic field components are included, in a WKB sense, explicitly in D through the plasma frequency, the thermal velocity and the cyclotron frequency. The equations in (1) give the variation in the (fast) phase, ψ, of the electric and magnetic fields of the ray along its characteristics.

The change in the amplitude of the electric field of the ray, $\vec{E}_0$ is determined in the following fashion.[8] The tensor $\overline{\overline{D}}^H$ can always be diagonalized by transforming to a new set of basis vectors such that:

$$\overline{\overline{D}}^H = D_1\ \hat{e}_1\hat{e}_1^* + D_2\ \hat{e}_2\hat{e}_2^* + D_3\ \hat{e}_3\hat{e}_3^* \tag{4}$$

where D_1, D_2 and D_3 are the real eigenvalues and $\hat{e}_1, \hat{e}_2$, and $\hat{e}_3$ are the corresponding orthonormal, complex eigenvectors which form the set of new basis vectors. Then $D = det(\overline{\overline{D}}^H) = D_1 D_2 D_3$. In this new representation we can write:

$$\vec{E}_0 = A_1 \hat{e}_1 + A_2 \hat{e}_2 + A_3 \hat{e}_3 \tag{5}$$

Let us assume that along the IBW the dispersion relation $D = 0$ implies that $D_1 = 0$ while $D_2 \neq 0$ and $D_3 \neq 0$ (the nondegenerate case[8]). Since $\overline{\overline{D}}^H \cdot \vec{E}_0 = 0$, it follows that $A_2 = 0$ and $A_3 = 0$ so that $\hat{e}_1$ is the polarization vector of the IBW. The expressions for D_1 and $\hat{e}_1$ for the IBW are given in Appendix I. The evolution of the amplitude $|A_1|$ (the variation of the slow phase of A_1 will be ignored) along the ray trajectories (1) is given by:[8]

$$\frac{dU}{dt} + U \nabla \cdot \left(\frac{\partial \omega(\vec{k}(\vec{r}), \vec{r})}{\partial \vec{k}} \right) + \overline{\overline{\sigma}}^H : \vec{e_1} \vec{e_1}^* |A_1|^2 = 0 \tag{6}$$

where U is the wave energy density and $\overline{\overline{\sigma}}^H$ is the hermitian part of the conductivity tensor. It is important to note that the derivation of (6) is restricted to a weakly dissipative wave: the dissipated power density (the last term in (6)) is assumed to be of the same order as the slow variation in the wave energy density.[11] The derivative with respect to t in (6) is along the ray paths given by (1). The relation between U and A_1 is:

$$U = \frac{1}{8\pi} \frac{\partial(\omega D_1)}{\partial \omega} |A_1|^2 \tag{7}$$

The second and third terms in (6) describe changes in U due to the convergence and divergence of a bundle of rays and due to the absorption of wave energy by the plasma, respectively. The exact form of the second term in toroidal coordinates is given in Appendix II. In order to determine the second term in (6), it is necessary to evaluate the variation of the dyadic $\nabla \vec{k}$ along the ray trajectories. These evolution equations are also given in Appendix II. Consequently, the evolution of the amplitude, $|A_1|$, requires the simultaneous solution of the six ray trajectory equations (1), the wave energy density equation (6) and the six equations for the dyadic $\nabla \vec{k}$ (Appendix II).

The ray paths in the phase space are completely determined by (1) for any initial values of $\vec{k}$ and $\vec{r}$. However, to determine the evolution of $|A_1|$ not only requires the initial

value of $|A_1|$ but also the initial values of the variations of $\vec{k}$ with respect to $\vec{r}$. These values are trivial if the rays are launched in a vacuum where $\nabla\vec{k}$ is identically zero. In the case of interest to us, the rays corresponding to an IBW are initiated somewhere inside the plasma just after the mode conversion of a fast Alfvén wave. There one can determine the initial values of $\nabla\vec{k}$ only if the constant phase (i.e. constant ψ) surface is explicity known. Without this knowledge it is not possible to know exactly the initial values of $\nabla\vec{k}$. The construction of the constant ψ surface inside the plasma will require the evolution of the known constant ψ surface at the antenna along the fast Alfvén waves and through the mode conversion region. This is further complicated by the fact that, since the excitation frequency is below the plasma frequency, there is a cut-off region near the edge of the plasma through which the antenna fields have to tunnel before exciting the propagating fast Alfvén wave. This whole process of constructing the constant ψ surface, which is beyond the mode conversion region and is the starting point for the IBW, is a formidable one and beyond the scope of the present work. We shall be getting back to this point when we discuss the effect of focusing on the evolution of A_1 along the rays.

III. NUMERICAL EVALUATION OF RAY TRAJECTORIES

The numerical code developed for solving the ray and amplitude equations is for a toroidal plasma whose constituents are described by their full Maxwellian distribution function.[7] The derivatives of the dielectric tensor elements have been explicitly determined (and checked using Macsyma) in order to avoid any errors due to numerical differentiation. While the code can be used for studying ray paths corresponding to any excitation frequency, we have utilized it, in its entirety, for studying the propagation of mode converted ion-Bernstein waves. Towards this end we have used parameters and profiles corresponding to a large tokamak (JET-type[1]) as described below. It should be emphasized that our choice of parameters is not intended to represent any particular experimental conditions. However, the parameters are in the general range that is typical of present-day tokamaks heated by externally applied RF power in the ion-cyclotron range of frequencies. Furthermore, these parameters are used to generate numerical results that guide the development and check the predictions of simple scaling models which describe the observed behavior

and can be extended to understand, in general, the propagation and damping of mode converted IBW's. Furthermore, the code itself can be used to study ray propagation for any sets of parameters and profiles other than the ones used in our analyses. We have assumed an axisymmetric toroidal equilibrium so that the toroidal mode number, n, remains constant along the rays. The magnetic field is assumed to be:

$$B_r = 0, \qquad B_\theta = 0.2\frac{I_p}{r}\frac{1 - exp(-\alpha_q r^2/a^2)}{(1 - exp(-\alpha_q))(1 + (r/R)cos\theta)}, \qquad B_\phi = \frac{B_{\phi 0}}{1 + \frac{r}{R}cos\theta} \tag{8}$$

where I_p is the plasma current in amperes, $\alpha_q = a/r_1 + 0.5$ [15], r_1 is the radius of the $q = 1$ surface (q is the safety factor), a is the minor radius, and $B_{\phi 0}$ is the toroidal magnetic field on axis. The factor of 0.2 in the equation for B_θ is the conversion factor needed so that B_θ is in Gaussian units when the toroidal current is measured in amperes and the distances are measured in centimeters. The density and temperature profiles are taken to be:

$$n_{e,i} = n_{e0,i0}\left(1 - \frac{r^2}{a^2}\right)^{3/2}, \quad T_e = T_{e0}exp\left(-\alpha_t\frac{r^2}{a^2}\right), \quad T_i = T_{i0}\left(1 - \frac{r^2}{a^2}\right)^{3/2} \tag{9}$$

where n_{e0}, n_{i0} are the electron and ion densities on axis, respectively, T_{e0}, T_{i0} are the electron and ion temperatures on axis, respectively, and $\alpha_t = 2\alpha_q/3$.[15] For our numerical analyses we have assumed a deuterium-hydrogen plasma with hydrogen density being 4% of the deuterium density and both ion species having the same profiles with $T_{i0} = 1.7\ keV$. Also, we assume that: $n_{e0} = 2.8 \times 10^{13}\ cm^{-3}$, $T_{e0} = 1.8\ keV$, $B_{\phi 0} = 2\ Tesla$, $a = 125\ cm$, $R = 300\ cm$, $r_1 = 50\ cm$, and that, without loss of generality, the rays start at $\phi = 0$. In all the numerical runs, the rays are started from the high-field side of the mode conversion region where the IBW is a propagating mode. The full dispersion relation is solved for k_r at the starting point for given values of the poloidal mode number, m, and $k_\parallel$. The toroidal mode number, n, is determined from (2). The rays are followed using (1) and (6) until either the wave energy density, U, is $\lesssim 10^{-4}$ of its initial starting value, or the rays have reached near the edge of the plasma. For the results discussed here we have excluded the effect of the second term in (6), i.e. we have ignored the focusing/defocusing effects,

but retained the damping term. The effect of the focusing term on the evolution of A_1 will be discussed in Section VI.

Figure 1a shows the poloidal projection of the ray trajectories for three rays starting at different locations with the wave frequency being $\omega = 1.58 \times 10^8 sec^{-1}$. The lines labeled C and I are the locations of the cyclotron resonance ($\omega = 2\omega_{cd} = \omega_{ch}$; ω_{cd} and ω_{ch} being the cyclotron frequencies of deuterium and hydrogen, respectively) and the cold plasma ion-ion hybrid resonance layers, respectively. The corresponding change in ϕ as a function of ωt (the normalized time of propagation along the ray) is shown in Fig. 1b. The rays which are started closer to the equatorial axis propagate further into the plasma, both radially and toroidally, before the amplitude, $|A_1|$, as shown in Fig. 1c, damps away. The reason for damping is the enhancement in $|m|$ along the rays as shown in Fig. 1d. From (2) it is clear that this increase in $|m|$ gives an upshift in $k_\parallel$. As a consequence, the Landau resonance parameter for the electrons, $y_{0e} = \omega / \left(\sqrt{2}|k_\parallel| v_{te}\right)$ ($v_{te} = \sqrt{\kappa T_e / m_e}$ is the electron thermal velocity), as shown in Fig. 1e, decreases from being > 3 to ≈ 1 just in the region where $|A_1|$ decreases substantially (Fig. 1c). Clearly this implies that the wave energy and momentum have been transferred to the electrons. Prior to the time when electron Landau damping becomes important, the energy density, U, does not change. The corresponding changes in $|A_1|$ (Fig. 1c) are primarily due to the dispersive properties of the plasma as evidenced in (7). The hash marks intersecting the ray trajectories in Fig. 1a indicate the point after which Landau damping starts to affect $|A_1|$. This corresponds to $\omega t \approx 293$ for ray 1, while for rays 2 and 3 this corresponds to the time when $|A_1|$ reaches its maximum value.

Figure 1d shows that the rate of change of $|m|$ increases as the starting position of the rays is moved away from the equatorial plane. Furthermore, as is evident for ray 3, the rate of change of $|m|$ increases as the ray propagates away from the equatorial plane. The change in the slope of m for ray 3 at $\omega t \approx 900$ (Fig. 1d) occurs just after the ray crosses the mid-plane and rotates towards decreasing θ (Fig. 1a). However, as is obvious from Figs. 1a and 1d, once Landau damping becomes significant, the rate of change of $|m|$ is not affected by the poloidal rotation of the ray.

For rays started below the equatorial plane, the trajectories in the poloidal plane are mirror images of the rays started above the equatorial plane. However, for the rays started

below the equatorial plane, the toroidal motion (along ϕ) is in the opposite direction to that for the rays started above the equatorial plane, and the increase in m is towards positive values. This is a general feature of IBW's for all ranges of parameter values.

An interesting effect takes place when the plasma current is reduced to 500 kA. This is evident in Fig. 2 where the rays are started at almost the same location as in Fig. 1a. Here the rays propagate much further away from the mode conversion region than in the case of the higher plasma current before transferring their energy to the electrons. The increase in $|m|$ is found to be substantially (three to six times) larger than in the previous case (Fig. 1d).

As the plasma current is reduced further, the rays tend to propagate further out towards the edge of the plasma and may not damp inside the plasma. In the limit of zero plasma current the rays do not damp at all inside the plasma but propagate straight out to the edge region. Even in this case $|m|$ increases substantially (almost at the same rate as in the case of non-zero toroidal current) but, as is obvious from (2), there is no corresponding change in $k_{\|}$.

If we increase ω to $1.93 \times 10^8\ sec^{-1}$, the cyclotron resonance, $\omega = 2\omega_{cd}$, layer is closer to the mid-plane. Here, for $I_p = 2\ MA$, the essential features of the rays are similar to those in Fig. 1. The only difference is that the rays propagate further out towards the edge of the plasma before damping. However, if we reduce I_p to 500 kA it is clearly evident from Figs. 3a and 3b that the ray which is started closer to the equatorial plane (ray 3) has not damped as it propagates out to the plasma edge. The amplitude, $|A_1|$ along ray 3 continues to increase monotonically (Fig. 3b). This occurs in spite of the fact that $|m|$ increases to approximately seven times the value of $|m|$ for ray 3 in Fig. 1d. The values of $|m|$ for rays 1 and 2 also increase to about seven times the values attained for rays 1 and 2 in Fig. 1d.

From the numerically generated results we arrive at the following basic properties of the IBW propagation in toroidal plasmas. IBW rays started nearer to the equatorial plane propagate longer distances away from the ion-ion hybrid resonance layer before they damp (if they do damp at all) than rays started further away from the equatorial plane. The distance of propagation increases as the toroidal current (or $|B_\theta|$) is decreased. As

the $\omega = 2\omega_{cd}$ resonance layer is moved towards the higher field side the IBW's propagate further out towards the edge of the plasma. The poloidal mode number, m, increases towards larger negative values for rays in the upper half plane and towards larger positive values for rays in the lower half plane. The increase in $|m|$ occurs even when there is no toroidal current ($B_\theta = 0$). This enhancement in m and a finite toroidal current are necessary for damping of the IBW. If the IBW's do damp, they impart their energy, through Landau damping, to the electrons.

IV. ANALYSIS OF RESULTS

While the numerical results obtained above have been for the full dielectric tensor of a Maxwellian plasma, some of the more important numerical observations can be understood in terms of a simple dispersion relation describing the IBW. The simplified, approximate dispersion relation for the IBW is given by (Appendix III):

$$D^{IB} \approx n_\perp^2 + \frac{a_0}{a_1} = 0 \tag{10}$$

where

$$\begin{aligned} a_0 &= 1 - n_\parallel^2 - \frac{\omega_{pd}^2}{\omega^2}\left(\frac{\omega^2}{\omega^2 - \omega_{cd}^2} + 2\eta\frac{\omega^2}{\omega^2 - \omega_{ch}^2}\right) \\ a_1 &= \epsilon\left(\frac{\omega^2}{\omega^2 - \omega_{cd}^2} - \frac{\omega^2}{\omega^2 - \omega_{ch}^2}\right) \\ \epsilon &= \frac{\omega_{pd}^2}{\omega_{cd}^2}\,\frac{v_{td}^2}{c^2} \end{aligned} \tag{11}$$

and $n_\parallel = ck_\parallel/\omega$, $n_\perp = ck_\perp/\omega$, ω_{cd} and v_{td} are the plasma frequency and thermal velocity of the deuterium ions, respectively, and η is the ratio of the hydrogen density to the deuterium density. In the sub-sections below we use this dispersion relation to examine some of the properties of the IBW and compare them with the numerical results of the previous section.

A. Radial group velocity

From (10) the radial motion (group velocity) of the IBW is given by:

$$\frac{dr}{dt} = -\frac{(\partial D^{IB}/\partial k_r)}{(\partial D^{IB}/\partial \omega)} = -2\left(\frac{ck_r}{\omega}\right)\frac{1}{(\partial D^{IB}/\partial \omega)} \tag{12}$$

where we have assumed that $B_r = 0$. Using (11) we find that along the IBW:

$$\frac{\partial D^{IB}}{\partial \omega} = \epsilon\frac{6}{a_1^2}\frac{\omega^5\omega_{cd}^2}{\left(\omega^2-\omega_{cd}^2\right)^2\left(\omega^2-4\omega_{cd}^2\right)^2}\left[5\frac{\omega_{cd}^2}{\omega^2}-2+n_\parallel^2\left(1-4\frac{\omega_{cd}^4}{\omega^4}\right)+\frac{\omega_{pd}^2}{\omega^2}(1+2\eta)\right] \tag{13}$$

The difference between $2\omega_{cd}$ and ω, relative to ω, is approximately the ratio of the distance of the IBW ray from the cyclotron resonance (where $\omega = 2\omega_{cd}$) to the major radius. By ignoring this difference we assume that $\omega \approx 2\omega_{cd}$ along the IBW. With this approximation it is easy to see that the right hand side of (13) is positive provided $\omega_{pd}^2 \gtrsim 3\omega_{cd}^2$. This indeed is the case for all the numerical results where the mode conversion region is near the center of the plasma. Thus, the sign of k_r in (12) determines the direction of the radial propagation of the IBW. Since the IBW propagates away from the mode conversion region (towards the high B-field side), rays that are started on the right side of the mid-plane require k_r to be positive while rays started on the left side of the mid-plane require k_r to be negative, i.e. $k_r dr < 0$. This is also consistent with the fact that the IBW is a backward wave. Consequently, for a ray which crosses the mid-plane k_r will change sign as the ray passes through the mid-plane. This is observed to be the case when we follow the IBW with our numerical code.

B. Poloidal group velocity

The ratio of the radial group velocity to the poloidal group velocity is:

$$\frac{dr}{d\theta} = \frac{(\partial D^{IB}/\partial k_r)}{(\partial D^{IB}/\partial m)} = \frac{k_r}{\left[\frac{m}{r^2}-\frac{k_\parallel}{r}\frac{B_\theta}{|B|}\left(1+\frac{1}{a_1}\right)\right]} \tag{14}$$

Since, near mode conversion, $k_\parallel$ and m are assumed to be very small it follows, from (3), that $|k_r| \approx |k_\perp| >> |k_\parallel|$. Thus, from (14), the radial group velocity is much larger than the poloidal group velocity. This is evident from Figs. 1a, 2 and 3a where, initially, the predominant group velocity of the IBW is in the radial direction. But, near the region

where Landau damping starts to play a role, the poloidal group velocity becomes larger than the radial group velocity. In this regime, our approximations for the dispersion relation in (10) are no longer valid (Appendix III).

C. Upshift of the poloidal mode numbers

The numerical results show that the electron Landau damping of the IBW occurs due to an upshift of $|m|$ which, in turn, for finite B_θ, leads to an upshift of $k_\parallel$. The change in m due to the radial motion of the IBW is given by (Appendix III):

$$\frac{dm}{dr} \approx \frac{4}{3} \frac{\omega_{cd}^2}{k_r v_{td}^2} \frac{r sin\theta}{(R + r cos\theta)} \tag{15}$$

The factor $r sin\theta / (R + r cos\theta)$ in (15) comes from the profiles of the magnetic fields given in (8). Equation (15) yields a very interesting property about IBW's. Since, from (12), $k_r dr < 0$, the change in m is always towards negative values in the upper half poloidal plane, $0 < \theta < \pi$, and towards positive values in the lower half poloidal plane. Consequently, IBW's in the upper half plane will shift towards negative parallel phase velocities before damping on the electrons while those in the lower half plane will shift towards positive parallel phase velocities before damping on the electrons. This is confirmed by the numerical solutions. Thus, IBW's are not suitable candidates for driving electron currents in tokamaks.

From (15) it is evident that, in order to have the same enhancement in $|m|$, rays which start closer to the equatorial plane will propagate farther than rays which start away from the equatorial plane. Once an IBW moves away from the equatorial plane (15) shows that $|m|$ will increase at a faster rate. This is exactly as observed, for instance, for ray 3 in Fig. 1d.

D. Electron Landau damping of the IBW

For finite B_θ, an increase in $|m|$ causes the electron Landau resonance parameter, y_{0e}, to decrease. Numerical results show that the IBW damps on the electrons when $y_{0e} \sim 1$. Below, we evaluate an approximate measure of the distance of propagation of the IBW before it Landau damps on the electrons. This analysis is valid for rays which propagate short distances (compared to the minor radius) and in a region where the plasma parameters do not vary significantly over those distances.

If we assume that $|k_r| \approx |k_\perp|$, $\omega_{pd}/\omega >> |n_\parallel|$ then, from (10) and (11):

$$|k_r| \approx \frac{\omega_{cd}}{v_{td}} \left(\frac{\frac{8}{3} - 2\eta\delta}{2+\delta} \right) \approx \frac{8}{3\delta} \frac{\omega_{cd}}{v_{td}} \tag{16}$$

where $\delta = -\omega/(\omega - 2\omega_{cd})$, and we have assumed that $\omega \approx 2\omega_{cd}$ (Appendix III). δ is approximately the ratio of the major radius to the distance of a point on the IBW ray from the $\omega = 2\omega_{cd}$ layer. Typically, we find that $\delta > 10$. Substituting (16) into (15) gives:

$$\frac{dm}{dr} \approx \frac{32}{9\delta} \frac{\omega_{cd}}{v_{td}} \frac{r sin\theta}{R + r cos\theta} \text{ sign}(k_r) \tag{17}$$

From (3):

$$\frac{dk_\parallel}{dr} \approx \frac{1}{r} \frac{dm}{dr} \frac{B_\theta}{|B|} \tag{18}$$

where we have ignored the variation of the magnetic field with respect to r and assumed that, initially, $|n_\parallel|$ is small. Combining (17) and (18) gives:

$$\frac{dk_\parallel}{dr} \approx \frac{3\delta}{8} \frac{\omega_{cd}}{v_{td}} \frac{sin\theta}{R} \frac{B_\theta}{|B|} \text{ sign}(k_r) \tag{19}$$

By assuming that the right hand side of (19) varies slowly with respect to r, and that, initially, $k_\parallel = 0$, then to obtain $y_{0e} \sim 1$ requires a radial distance of propagation that is, approximately, given by:

$$\Delta r \approx \frac{8}{3\delta} \frac{\omega}{\omega_{cd}} \frac{|B|}{B_\theta} \frac{v_{td}}{v_{te}} \frac{R}{sin\theta} \tag{20}$$

This equation implies that the radial distance of propagation for the Landau damping of the IBW depends on $\sqrt{T_d/T_e}$. This is indeed confirmed by our numerical results. In Fig. 4 we have plotted the radial distance of propagation of the IBW as a function of ωt for three different scenarios:

(1) $T_{e0} = 5keV$, $T_{i0} = 5keV$

(2) $T_{e0} = 5keV$, $T_{i0} = 3keV$

(3) $T_{e0} = 1.8keV$, $T_{i0} = 1.7keV$ which is the same case as ray 2 in Fig. 1a.

In all three cases the rest of the parameters and all the profiles are taken to be the same as discussed in Section III. All the rays are for the case of $\omega = 1.58 \times 10^8 sec^{-1}$ (Fig. 1) and start at $\theta = 0.07\pi$ but at slightly different radial positions since the mode conversion region changes due to a change in temperatures. The rays are followed until $y_{0e} \approx 1.1$. The corresponding radial distances of propagation, as measured from Fig. 4, for the three cases are, approximately, $40.6cm$, $29.6cm$, and $42.5cm$, respectively. These distances are in the ratio of 1 : 0.73 : 1.06, respectively. However, for the three different temperature scenarios, equation (20) implies that the distances of propagation for the rays to reach $y_{0e} \sim 1.1$ should be approximately in the ratio 1 : 0.77 : 0.97, respectively. This is in fairly good agreement with the numerically observed ratios of the distances of propagation. This agreement is in spite of the fact that the rays propagate over significant distances that seriously test the validity of the approximations used in deriving (20).

Thus, the radial distances of propagation of IBW's, before damping on electrons, remain essentially the same if the electron and ion temperatures are increased but kept in the same ratio. However, if the electron temperature is greater than the ion temperature the distance of propagation decreases relative to the case when the two temperatures are the same. Consequently, if electron heating occurs the damping of the IBW on electrons will persist.

From (20) the distance of propagation, before damping, is inversely proportional to $sin\theta$ and B_θ. The former dependence indicates that rays nearer the equatorial plane propagate farther than those further away from the equatorial plane. The latter dependence implies that increasing the toroidal current will decrease the distance of propagation before damping of the IBW. This dependence on B_θ is borne out by the computations when the rays do not propagate over very large distances before damping sets in. In the case of Figs. 1a and 2, for ray (1), (20) would require that the IBW in Fig. 2 propagate four times the distance in Fig. 1a. The measured ratio is approximately 3 : 1. We have usually found that (20) gives values of distances of propagation which are within less than a factor of two of the exact numerical results even when the rays propagate over distances which are a significant fraction of the minor radius.

E. Toroidal group velocity

The ratio of the toroidal to the poloidal group velocities of the IBW is given by:

$$\frac{d\phi}{dr} = \frac{\partial D^{IB}/\partial n}{\partial D^{IB}/\partial k_r} = \frac{1}{k_r}\left\{\frac{n}{(R+rcos\theta)^2} - \frac{k_\parallel}{(R+rcos\theta)}\frac{B_\phi}{|B|}\left(1+\frac{1}{a_1}\right)\right\} \qquad (21)$$

where we have used the dispersion relation in (10). Since $a_1 > 0$ and $k_r dr < 0$, if n is positive and $k_\parallel$ negative then (21) implies that the rays will propagate towards negative values of ϕ. This is the case in Fig. 1b where $k_\parallel$ becomes negative, as m quickly becomes negative along the ray, and n was initially taken to be positive. Since we have assumed that the plasma parameters do not depend on ϕ, n remains a constant along the rays. Furthermore, from (21), the toroidal group velocity is small compared to the radial group velocity. This is exactly as observed in Figs. 1a and 1b.

V. FOCUSING OF RAYS

For the numerical results considered so far we have excluded the effect of focusing of rays on the evolution of the electric field amplitude, i.e. we have ignored the second term in (6) when solving for $|A_1|$. This, as mentioned earlier, is due to our inability to construct a surface of constant ψ from where the IBW's can be launched. In spite of this limitation, in this section we briefly describe the effect of keeping the second term in (6) on the evolution of $|A_1|$.

In Fig. 5 we have plotted $|A_1|$ along the trajectories of rays 1 and 2 of Fig. 1a with the second term included in (6). Here we have assumed that all the elements of the dyadic $\nabla\vec{k}$ are initially zero. There are no significant differences between Fig. 5 and Fig. 1c. We find that $|A_1|$ has a slightly larger value in Fig. 5 than in Fig. 1c, before damping, and that the amplitude decays away somewhat earlier in Fig. 5 than in Fig. 1c.

In Fig. 6 we plot two rays in the neighborhood of ray 1 of Fig. 1a. The rays essentially remain parallel to each other. However, as seen in Fig. 6, rays in the vicinity of ray 3 in Fig. 1a are highly focused as they pass the mid-plane before diverging near the damping region. This focusing of rays as they cross the mid-plane leads to the higher value of $|A_1|$ for ray 2 in Fig. 5 than in Fig. 1c, while for ray 1, which does not cross the mid-plane

before damping, $|A_1|$ in Fig. 1a and Fig. 5 are almost the same. The strong focusing of ray 3 near the mid-plane causes some numerical difficulties whereby our numerical integration scheme does not converge properly. But, the evolution of $|A_1|$ for ray 3 can be qualitatively deduced from the above observations on rays 1 and 2. We expect that, for ray 3, $|A_1|$ will enhance substantially over that given in Fig. 1c, as the ray crosses the mid-plane, but, once Landau damping takes over, ray 3 should damp close to the location shown in Fig. 1a.

Thus, we conclude that, even when the second term in (6) is kept in the equation for the evolution of $|A_1|$, there will be no significant changes to the results already obtained in Section III.

It should be pointed out that one can continue to solve (6) without including the second term provided one follows the trajectories of a bundle of rays launched from an initial surface. A change in the cross-sectional area at subsequent times would give a change in the energy density, U, due to the focusing effect. The concurrent change in $|A_1|$ then can be calculated from (7).

VI. CONCLUSIONS

We have presented a detailed numerical and analytical study of the propagation of ion-Bernstein waves generated by mode conversion of the FAW in ICRF heating of tokamak plasmas. The poloidal mode numbers are greatly enhanced along the IBW's but the Landau damping of the IBW's is dependent on the magnitude of the toroidal current (or, equivalently, the poloidal magnetic field). If the mode converted IBW's damp, then they Landau damp their energy on the electrons. However, these IBW's cannot drive electron currents in the plasma since they impart their energy (and momentum) to electrons with negative parallel phase velocities in the upper half poloidal plane and to electrons with positive parallel phase velocities in the lower half poloidal plane. The damping of the IBW is dependent on the ratio of the electron to the ion temperatures. The distance of propagation of the IBW before it damps is inversely proportional to the square-root of this ratio. Also, IBW's closer to the equatorial plane propagate longer distances before damping than IBW's further away from the equatorial plane.

ACKNOWLEDGEMENTS

We thank Prof. I. Bernstein for discussions on certain aspects of ray tracing. This work was supported in part by U.S. Department of Energy Contract No. DE-AC02-78ET-51013 and in part by National Science Foundation Grant No. ECS-88-2475.

APPENDIX I

The relationship between the hermitian part of the dielectric tensor, $\overline{\overline{D}}^H$, and the anti-hermitian part of the conductivity tensor, $\overline{\overline{\sigma}}^A$, is given by:

$$\overline{\overline{D}}^H = \left(1 - \frac{c^2k^2}{\omega^2}\right)\overline{\overline{I}} + \frac{c^2}{\omega^2}\vec{k}\vec{k} + \frac{4\pi i}{\omega}\overline{\overline{\sigma}}^A \qquad (A1.1)$$

where $\overline{\overline{I}}$ is the identity tensor. The eigenvalues, D_1, D_2, D_3, correspond to the three roots of the cubic equation (in λ): $det(\overline{\overline{D}}^H - \lambda\overline{\overline{I}}) = 0$. By expressing $\overline{\overline{D}}^H$ in terms of its elements as in (10), the eigenvalues can be explicitly evaluated in terms of these elements.[16] We find, numerically, that for the parameters of the IBW satisfying the dispersion relation $D = D_1D_2D_3 = 0$, there exists only one eigenvalue D_1 which is zero while the other two, D_2, D_3, remain non-zero. This eigenvalue corresponding to the IBW is given by:

$$\lambda_{IB} \;=\; D_1 \;=\; s_+ + s_- - \frac{q_2}{3} \qquad (A1.2)$$

where:

$$\begin{aligned} s_\pm &= \left[p_1 \pm \sqrt{p_2^3 + p_1^2}\right]^{1/3} \\ p_1 &= \frac{q_1}{3} - \left(\frac{q_2}{3}\right)^2 \\ p_2 &= \frac{1}{6}(q_1q_2 - 3q_0) - \left(\frac{q_2}{3}\right)^3 \end{aligned} \qquad (A1.3)$$

with q_0, q_1 and q_2 given by:

$$\begin{aligned} q_0 &= -\,det(\overline{\overline{D}}^H) \\ q_1 &= D_{11}(D_{22} + D_{33}) + D_{22}D_{33} + D_{12}^2 - D_{13}^2 + D_{23}^2 \\ q_2 &= -\,trace(\overline{\overline{D}}^H) \end{aligned} \qquad (A1.4)$$

Here we have expressed $\overline{\overline{D}}^H$ in terms of its tensor elements:

$$\overline{\overline{D}}^H = \begin{pmatrix} D_{11} & D_{12} & D_{13} \\ -D_{12} & D_{22} & D_{23} \\ D_{13} & -D_{23} & D_{33} \end{pmatrix} \qquad (A1.5)$$

The polarization of the IBW is:

$$\hat{e}_1 = f_0 \begin{pmatrix} 1 \\ f_1 \\ f_2 \end{pmatrix} \tag{A1.6}$$

where:

$$f_1 = \frac{D_{12}D_{13} + D_{23}\left(D_{11} - \lambda_{IB}\right)}{D_{13}\left(D_{22} - \lambda_{IB}\right) - D_{12}D_{23}}$$

$$f_2 = -\frac{D_{12}^2 + \left(D_{11} - \lambda_{IB}\right)\left(D_{22} - \lambda_{IB}\right)}{D_{13}\left(D_{22} - \lambda_{IB}\right) - D_{12}D_{23}} \tag{A1.7}$$

$$f_0 = \frac{1}{\left(1 + f_1^2 + f_2^2\right)}$$

These formulas for D_1 and $\hat{e}_1$ are used in (6) and (7) to solve for the evolution of the amplitude of the electric field along the ray trajectories.

APPENDIX II

The relationship between the Cartesian and the toroidal coordinate systems is:

$$\begin{aligned} x &= (R + r\ cos\theta)\ cos\phi \\ y &= r\ sin\theta \\ z &= (R + r\ cos\theta)\ sin\phi \end{aligned} \tag{A2.1}$$

and the relationship between the Cartesian and toroidal wave numbers is:

$$\begin{aligned} k_x &= k_r\ cos\theta\ cos\phi - \frac{m}{r}\ sin\theta\ cos\phi - \frac{n}{(R + r cos\theta)}\ sin\phi \\ k_y &= k_r\ sin\theta + \frac{m}{r}\ cos\theta \\ k_z &= k_r\ cos\theta\ sin\phi - \frac{m}{r}\ sin\theta\ sin\phi + \frac{n}{(R + r\ cos\theta)}\ cos\phi \end{aligned} \tag{A2.2}$$

It is then easy to show that:

$$\nabla \cdot \left(\frac{\partial \omega\left(\vec{k}(\vec{r}), \vec{r}\right)}{\partial \vec{k}} \right) = \frac{1}{J}\ \frac{\partial}{\partial x_i} \left(J\ \frac{\partial}{\partial k_i} \omega\left(\vec{k}(\vec{r}), \vec{r}\right) \right) \tag{A2.3}$$

where $J = r(R + rcos\theta)$ is the Jacobian of the coordinate transformation, $(x_1, x_2, x_3) = (r, \theta, \phi)$, $(k_1, k_2, k_3) = (k_r, m, n)$, and a sum over repeated indices (from 1 to 3) is implied. In the above equation the derivatives with respect to x_i correspond to the explicit and implicit (through $\vec{k}$) dependencies of $\omega(\vec{k}(\vec{r}), \vec{r})$ on x_i. The above equation can be re-expressed in terms of $D(\vec{k}, \omega, \vec{r})$:

$$\nabla \cdot \left(\frac{\partial \omega(\vec{k}(\vec{r}), \vec{r})}{\partial \vec{k}} \right) = - \frac{1}{\partial D/\partial \omega} \left[\frac{1}{J} \frac{\partial J}{\partial x_i} \frac{\partial D}{\partial k_i} + \left\{ \frac{\partial^2 D}{\partial x_i \partial k_i} - \frac{\partial^2 D}{\partial x_i \partial \omega} \frac{\partial D/\partial k_i}{\partial D/\partial \omega} \right\} + \left\{ \frac{\partial^2 D}{\partial k_i \partial k_j} - \frac{\partial^2 D}{\partial k_j \partial \omega} \frac{\partial D/\partial k_i}{\partial D/\partial \omega} \right\} \frac{\partial k_j}{\partial x_i} \right] \tag{A2.4}$$

where, now, the derivatives with respect to x_i correspond to the explicit dependence of D on x_i. In (A2.4) the evolution of $\partial k_j/\partial x_i$ along the rays is the only quantity that needs to be determined. This is given by:[8]

$$\frac{d}{dt} \left(\frac{\partial k_i}{\partial x_j} \right) = - \frac{\partial^2 \omega}{\partial x_i \partial x_j} - \frac{\partial^2 \omega}{\partial x_j \partial k_l} \frac{\partial k_l}{\partial x_i} - \frac{\partial^2 \omega}{\partial x_i \partial k_l} \frac{\partial k_j}{\partial x_l} - \frac{\partial^2 \omega}{\partial k_p \partial k_l} \frac{\partial k_j}{\partial x_l} \frac{\partial k_p}{\partial x_i} \tag{A2.5}$$

where, again, the derivatives with respect to x_i correspond to the explicit dependencies, and the derivative with respect to t is along the ray trajectories given by (1). The derivatives of ω can be replaced by derivatives of D by either using the following relations or applying the chain rule to them:

$$\frac{\partial \omega}{\partial x_i} = - \frac{\partial D/\partial x_i}{\partial D/\partial \omega} \ , \qquad \frac{\partial \omega}{\partial k_i} = - \frac{\partial D/\partial k_i}{\partial D/\partial \omega} \tag{A2.6}$$

where all the derivatives are with respect to the explicit dependencies. Since $\nabla \times \vec{k} = 0$, there are only six independent elements of the dyadic $\nabla \vec{k}$ that need to be evaluated along the ray trajectories by (A2.5). This completes the determination of the second term in (6) corresponding to the focusing (or de-focusing) of rays.

APPENDIX III

The approximate dispersion relation is derived by expanding the dielectric tensor elements for the Maxwellian plasma[7] to order $(k_\perp \rho_s)^4$ for all the plasma species. (Here

$s = (h, d, e)$ is the species index for hydrogen, deuterium and electrons, respectively, and ρ_s is the appropriate Larmor radius.) By further assuming that the hydrogen ion density is very small compared to the deuterium ion density, that $\omega_{pe} \gg \omega \sim \omega_{cd}$, and that the density and temperature profiles are the same for all the species, we obtain the following approximate forms for the required tensor elements:

$$\begin{aligned}
D_{11} &\approx a_0 + a_1 n_\perp^2 + a_2 n_\perp^4 \\
iD_{12} &\approx c_0 + c_1 n_\perp^2 + c_2 n_\perp^4 \\
D_{13} &\approx d_1 n_\perp + d_2 n_\perp^3 \\
D_{22} &\approx a_0 + b_1 n_\perp^2 + b_2 n_\perp^4 \\
iD_{23} &\approx g_1 n_\perp + g_2 n_\perp^3 \\
D_{33} &\approx 2\frac{\omega_{pe}^2}{\omega^2} y_{0e}^2 \left\{ 1 + y_{0e} Z\left(y_{0e}\right) \right\}
\end{aligned} \tag{A3.1}$$

where:

$$\begin{aligned}
a_0 &= 1 - n_\parallel^2 + \frac{1}{2}\,\frac{\omega_{pd}^2}{\omega^2}\,\left(w_{1d}^+ + 2\eta w_{1h}^+\right) \\
a_1 &= \frac{1}{2}\,\frac{\omega_{pd}^2}{\omega_{cd}^2}\,\frac{v_{td}^2}{c^2}\,\left(-w_{1d}^+ + w_{2d}^+\right) \\
a_2 &= \frac{1}{2}\left(\frac{\omega_{pd}\omega}{\omega_{cd}^2}\right)^2\,\frac{v_{td}^4}{c^4}\,\left(\frac{5}{8}w_{1d}^+ - w_{2d}^+ + \frac{3}{8}w_{3d}^+\right) \\
b_1 &= -1 + \frac{1}{2}\,\frac{\omega_{pd}^2}{\omega_{cd}^2}\,\frac{v_{td}^2}{c^2}\,\left(2w_{0d}^+ - 3w_{1d}^+ + w_{2d}^+ + 2(1+\eta)\frac{T_e}{T_d}w_{0e}^+\right) \\
b_2 &= \frac{1}{2}\left(\frac{\omega_{pd}\omega}{\omega_{cd}^2}\right)^2\,\frac{v_{td}^4}{c^4}\,\left(-3w_{0d}^+ + \frac{37}{8}w_{1d}^+ - 2w_{2d}^+ + \frac{3}{8}w_{3d}^+\right) \\
c_0 &= -\frac{1}{2}\,\frac{\omega_{pd}^2}{\omega^2}\,\left(w_{1d}^- + 2\eta w_{1h}^- - 2(1+\eta)\frac{\omega}{\omega_{cd}}\right) \\
c_1 &= -\frac{1}{2}\,\frac{\omega_{pd}^2}{\omega_{cd}^2}\,\frac{v_{td}^2}{c^2}\,\left(-2w_{1d}^- + w_{2d}^-\right) \\
c_2 &= -\frac{1}{2}\left(\frac{\omega_{pd}\omega}{\omega_{cd}^2}\right)^2\,\frac{v_{td}^4}{c^4}\,\left(\frac{15}{8}w_{1d}^- - \frac{3}{2}w_{2d}^- + \frac{3}{8}w_{3d}^-\right) \\
d_1 &= n_\parallel + \frac{1}{2n_\parallel}\,\mathrm{sign}\left(\mathrm{n}_\perp\right)\,\left(\frac{\omega_{\mathrm{pd}}^2}{\omega\omega_{\mathrm{cd}}}\right)\left(\mathrm{v}_{1\mathrm{d}}^- + \eta \mathrm{v}_{1\mathrm{h}}^-\right)
\end{aligned} \tag{A3.2}$$

$$d_2 = \frac{1}{2n_\parallel}\,\mathrm{sign}\,(\mathrm{n}_\perp)\left(\frac{\omega_{\mathrm{pd}}^2\omega}{\omega_{\mathrm{cd}}^3}\right)\frac{\mathrm{v}_{\mathrm{td}}^2}{\mathrm{c}^2}\left(-\mathrm{v}_{1\mathrm{d}}^- + \frac{1}{2}\mathrm{v}_{2\mathrm{d}}^-\right)$$

$$g_1 = \frac{1}{2n_\parallel}\,\mathrm{sign}\,(\mathrm{n}_\perp)\left(\frac{\omega_{\mathrm{pd}}^2}{\omega\omega_{\mathrm{cd}}}\right)\left\{-\mathrm{v}_{0\mathrm{d}}^+ + \mathrm{v}_{1\mathrm{d}}^+ + \eta\left(-\mathrm{v}_{0\mathrm{h}}^+ + \mathrm{v}_{1\mathrm{h}}^+\right) + (1+\eta)\left(2 + \mathrm{v}_{0\mathrm{e}}^+\right)\right\}$$

$$g_2 = \frac{1}{2n_\parallel}\,\mathrm{sign}\,(\mathrm{n}_\perp)\left(\frac{\omega_{\mathrm{pd}}^2\omega}{\omega_{\mathrm{cd}}^3}\right)\frac{\mathrm{v}_{\mathrm{td}}^2}{\mathrm{c}^2}\left\{3\mathrm{v}_{0\mathrm{d}}^+ - 4\mathrm{v}_{1\mathrm{d}}^+ + \mathrm{v}_{2\mathrm{d}}^+\right\}$$

In the above expressions:

$$w_{js}^{\pm} = y_{0s}\,\mathrm{Re}\left\{\mathrm{Z}\,(\mathrm{y}_{\mathrm{js}}) \pm \mathrm{Z}\,(\mathrm{y}_{-\mathrm{js}})\right\}$$

$$v_{js}^{\pm} = \mathrm{Re}\left\{\mathrm{y}_{\mathrm{js}}\mathrm{Z}\,(\mathrm{y}_{\mathrm{js}}) \pm \mathrm{y}_{-\mathrm{js}}\mathrm{Z}\,(\mathrm{y}_{-\mathrm{js}})\right\}$$

$$y_{\pm js} = \frac{\omega \mp j\omega_{cs}}{\sqrt{2}|k_\parallel|v_{ts}}$$

where $j = (0, 1, 2)$, and Z is the plasma dispersion function. In the expression for D_{33} we have retained only the electron contribution as that greatly dominates over the ion contributions.

In the initial propagation region of the rays where electron Landau damping is not important, $|D_{33}|$ is much greater than the magnitude of any other tensor element. This can be easily determined from (A3.1) and (A3.2). Then we can approximate the determinant of $\overline{\overline{D}}^H$ by:

$$\begin{aligned} D &\approx D_{11}D_{22} + D_{12}^2 \\ &\approx \alpha_2 n_\perp^4 + \alpha_1 n_\perp^2 + \alpha_0 \end{aligned} \tag{A3.3}$$

where the α's are given by:

$$\begin{aligned} \alpha_0 &= a_0^2 + c_0^2 \\ \alpha_1 &= a_0\,(a_1 + b_1) + 2c_0c_1 \\ \alpha_2 &= a_0\,(a_2 + b_2) + a_1b_1 + c_1^2 + 2c_0c_2 \end{aligned} \tag{A3.4}$$

The dispersion relation, obtained by setting $D = 0$, then gives two branches of $n_\perp^2$. One of them corresponds to the fast Alfvén wave and the other to the IBW. Away from the mode conversion region, where the two roots of $n_\perp^2$ are real, we find that the IBW is well represented by the dispersion relation:

$$D^{IBW} \approx n_\perp^2 + \frac{\alpha_1}{\alpha_2} = 0 \qquad (A3.5)$$

This can be further approximated into a simple form by replacing α_1 and α_2 by their most dominant terms in (A3.4). By realizing that:

$$\epsilon = \frac{\omega_{pd}^2}{\omega_{cd}^2}\frac{v_{td}^2}{c^2} << 1 \qquad (A3.6)$$

we find:

$$D^{IBW} \approx n_\perp^2 + \frac{a_0}{a_1} = 0 \qquad (A3.7)$$

The mode conversion region is to the high field side of the $\omega = 2\omega_{cd} = \omega_{ch}$ cyclotron resonance layer. The IBW becomes a propagating mode on the high-field side of the mode conversion layer. Consequently, the plasma dispersion functions in the dielectric tensor elements for the ions are asymptotically expanded and only the leading order non-vanishing terms are kept in a_0 and a_1. This gives:

$$\begin{aligned} a_0 &= 1 - n_\parallel^2 - \frac{\omega_{pd}^2}{\omega^2}\left(\frac{\omega^2}{\omega^2 - \omega_{cd}^2} + 2\eta\frac{\omega^2}{\omega^2 - \omega_{ch}^2}\right) \\ a_1 &= \epsilon\left(\frac{\omega^2}{\omega^2 - \omega_{cd}^2} - \frac{\omega^2}{\omega^2 - \omega_{ch}^2}\right) \end{aligned} \qquad (A3.8)$$

We have checked the solution to $n_\perp^2$ for the IBW obtained from (A3.7) and (A3.8) and find it to be in fair agreement with solution for the IBW obtained from the full dispersion tensor used in the computations for the ray trajectories. Thus, (A3.7) and (A3.8) become the basis of our analysis of the propagation of IBW and are used in Section IV.

The change in m due to a change in r along the ray trajectory is given by:

$$
\begin{aligned}
\frac{dm}{dr} &= -\frac{(\partial D^{IB}/\partial\theta)}{(\partial D^{IB}/\partial k_r)} \\
&= -\frac{n}{k_r}\left(\frac{n}{\omega\,(R+rcos\theta)} - k_{\|}\frac{B_\phi}{|B|}\right)\frac{rsin\theta}{(R+rcos\theta)^2} \\
&\quad -\frac{2}{\epsilon k_r\left(\delta+\frac{13}{6}\right)^2}\left[\left(\frac{\delta^2}{2}+\delta+\frac{83}{72}\right)\left(\frac{\omega^2}{c^2}-k_{\|}^2\right)-\left(\delta+\frac{13}{6}\right)\frac{n}{(R+rcos\theta)}\frac{B_\phi}{|B|}k_{\|}\right. \\
&\quad \left.+\frac{1}{2}\,\frac{\omega_{pd}^2}{c^2}\left\{-\frac{2}{3}\delta^2\,(2+\eta)-\frac{2}{9}\delta\,(16-7\eta)-5-\frac{11}{8}\eta\right\}\right]\;\frac{rsin\theta}{(R+rcos\theta)}
\end{aligned}
\tag{A3.9}
$$

In deriving (A3.9) we have made the following additional approximations:

$$
\frac{\omega}{\omega-\omega_{cd}}+\frac{\omega}{\omega+\omega_{cd}}\approx\frac{8}{3},\qquad \frac{\omega}{\omega+2\omega_{cd}}\approx\frac{1}{2} \tag{A3.10}
$$

which is the same as approximating ω by $2\omega_{cd}$ in the above expressions. Equation (A3.9) does not lend itself to an easy analysis. However, important aspects of the change in m with r can be determined by keeping the most dominant terms in (A3.9). This is done by realizing that $\epsilon \ll 1$, $\delta \gg 1$ and $\omega_{pd} \gg \omega$. Then, (A3.9) reduces to equation (15) in Section IV.

REFERENCES

[1] J. Jacquinot and the JET Team, Plasma Phys. Controlled Fusion **28**, 1 (1986).

[2] J. Jacquinot and JET Team, Plasma Phys. Controlled Fusion, **30**, 1467 (1988).

[3] P. Colestock, A. Cavallo, W. Dorland, J. Hosea, G. Greene, G. Hammett, H. W. Hendel, B. Howell, K. Jaehnig, R. Kaita, S. S. Medley, C. K. Phillips, A. L. Roquemore, G. Schilling, J. Stevens, B. Stratton, D. Smithe, A. Ramsey, G. Taylor, J. R. Wilson, S. J. Zweben, the TFTR Group, W. Gardner, and D. Hoffman, in *Applications of Radio-Frequency Power to Plasmas* edited by R. McWilliams (American Institute of Physics Conference Proceedings 190, New York, 1989) p. 189.

[4] D. G. Swanson, Phys. Fluids **28**, 2645 (1985).

[5] A. K. Ram and A. Bers, in *Applications of Radio-Frequency Power to Plasmas* edited by S. Bernabei and R. W. Motley (American Institute of Physics Conference Proceedings 159, New York, 1987) p. 402.

[6] A. K. Ram and A. Bers, in *Proceedings of the 1989 Conference on Plasma Physics*, edited by A. Sen and P. K. Kaw (New Delhi, India, 1989), Vol. I, p. 57.

[7] T. H. Stix, *The Theory of Plasma Waves* (McGraw-Hill, New York, 1962).

[8] I. B. Bernstein and L. Friedland, in *Handbook of Plasma Physics*, vol. 1, edited by M. N. Rosenbluth and R. Z. Sagdeev (North-Holland, New York, 1983), Vol. 1, pp. 367-418.

[9] A. H. Glasser and A. Bravo-Ortega, Phys. Fluids **30**, 797 (1987).

[10] V. Fuchs and A. Bers, Phys. Fluids **31**, 3702 (1988)

[11] A. Bers, in *Plasma Physics - Les Houches 1972*, edited by C. DeWitt and J. Peyraud (Gordon & Breach Science, 1975).

[12] R. K. Luneburg, *Mathematical Theory of Optics* (Brown University Lecture Notes, 1944); (republished by University of California Press, 1964).

[13] S. Weinberg, Phys. Rev. **126**, 1899 (1962).

[14] M. Kline and I. W. Kay, *Electromagnetic Theory and Geometrical Optics* (John Wiley, New York, 1965)

[15] W. M. Tang, Nucl. Fusion **26**, 1605 (1986).

[16] M. Abramowitz and I. A. Stegun, *Handbook of Mathematical Functions* (Dover Publications, New York, 1972).

FIGURE CAPTIONS

Figure 1a: The poloidal projection for three rays initially all started at $\phi = 0$ but with:

(1) $r = 61.94\ cm,\ \theta = 0.15\pi$

(2) $r = 55.63\ cm,\ \theta = 0.07\pi$

(3) $r = 54.07\ cm,\ \theta = 0.01\pi$.

Here $\omega = 1.58 \times 10^8\ sec^{-1}$, $I_p = 2\ MA$, $n_{\|} = 0.1$, the normalized poloidal mode number: $cm/\omega a = 0.01$, and the rest of the parameters are as given in the text. C is the location of the $\omega = 2\omega_{cd}$ resonance layer and I is the location of the cold plasma ion-ion hybrid resonance layer. $\tilde{x} = rcos\theta$, $\tilde{y} = rsin\theta$.

Figure 1b: The toroidal angle, ϕ, along the rays of Fig. 1a. ωt is the normalized time along the rays.

Figure 1c: The amplitude, $|A_1|$ along the rays of Fig. 1a. Here the initial amplitude is assumed to be one.

Figure 1d: The poloidal mode number, m, along the rays of Fig. 1a.

Figure 1e: The Landau resonance parameter for the electrons, y_{0e}, along the rays of Fig. 1a.

Figure 2: Same as Fig. 1a except that $I_p = 500\ kA$ and the rays are started at:

(1) $r = 55.69\ cm, \theta = 0.15\pi$

(2) $r = 50.46\ cm, \theta = 0.07\pi$

(3) $r = 49.18\ cm, \theta = 0.01\pi$

Figure 3a: Same as Fig. 2 except that $\omega = 1.93 \times 10^8\ sec^{-1}$ and the rays are started at:

(1) $r = 17.86\ cm,\ \theta = 0.8\pi$

(2) $r = 15.24\ cm,\ \theta = 0.9\pi$

(3) $r = 14.52\ cm,\ \theta = 0.99\pi$.

Figure 4: The variation of r along three rays with all parameters being the same as in Fig. 1a except that initially $\theta = 0.07\pi$ for all the rays and:

(1) $r = 50.07\ cm,\ T_{e0} = 5.0\ keV,\ T_{i0} = 5.0\ keV$

(2) $r = 53.36\ cm,\ T_{e0} = 5.0\ keV,\ T_{i0} = 3.0\ keV$

(3) $r = 55.63\ cm,\ T_{e0} = 1.8\ keV,\ T_{i0} = 1.7\ keV$

Figure 5: Following $|A_1|$ along rays 1 and 2 of Fig. 1a with the effects of focusing included in the equation for the evolution of $|A_1|$.

Figure 6: Poloidal projection of the rays in the neighborhood of rays 1 and 3 of Fig. 1a.

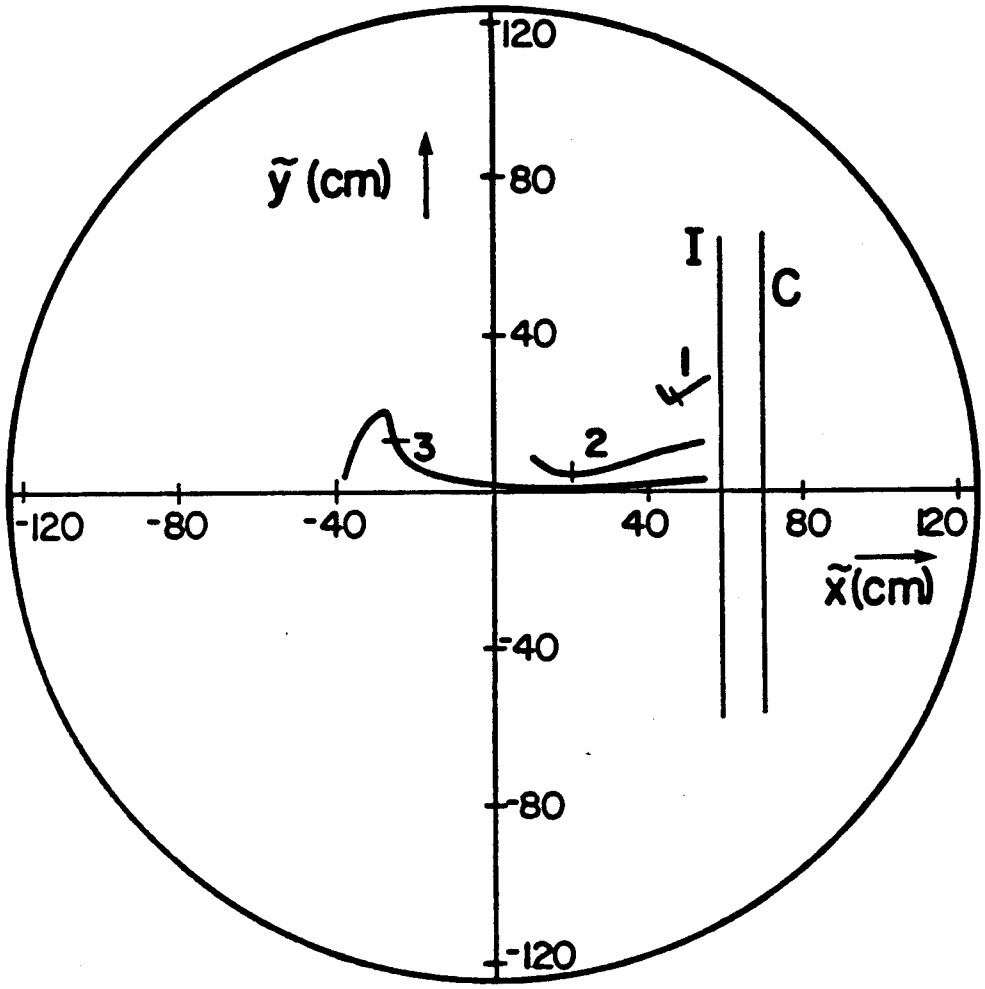

Figure 1a

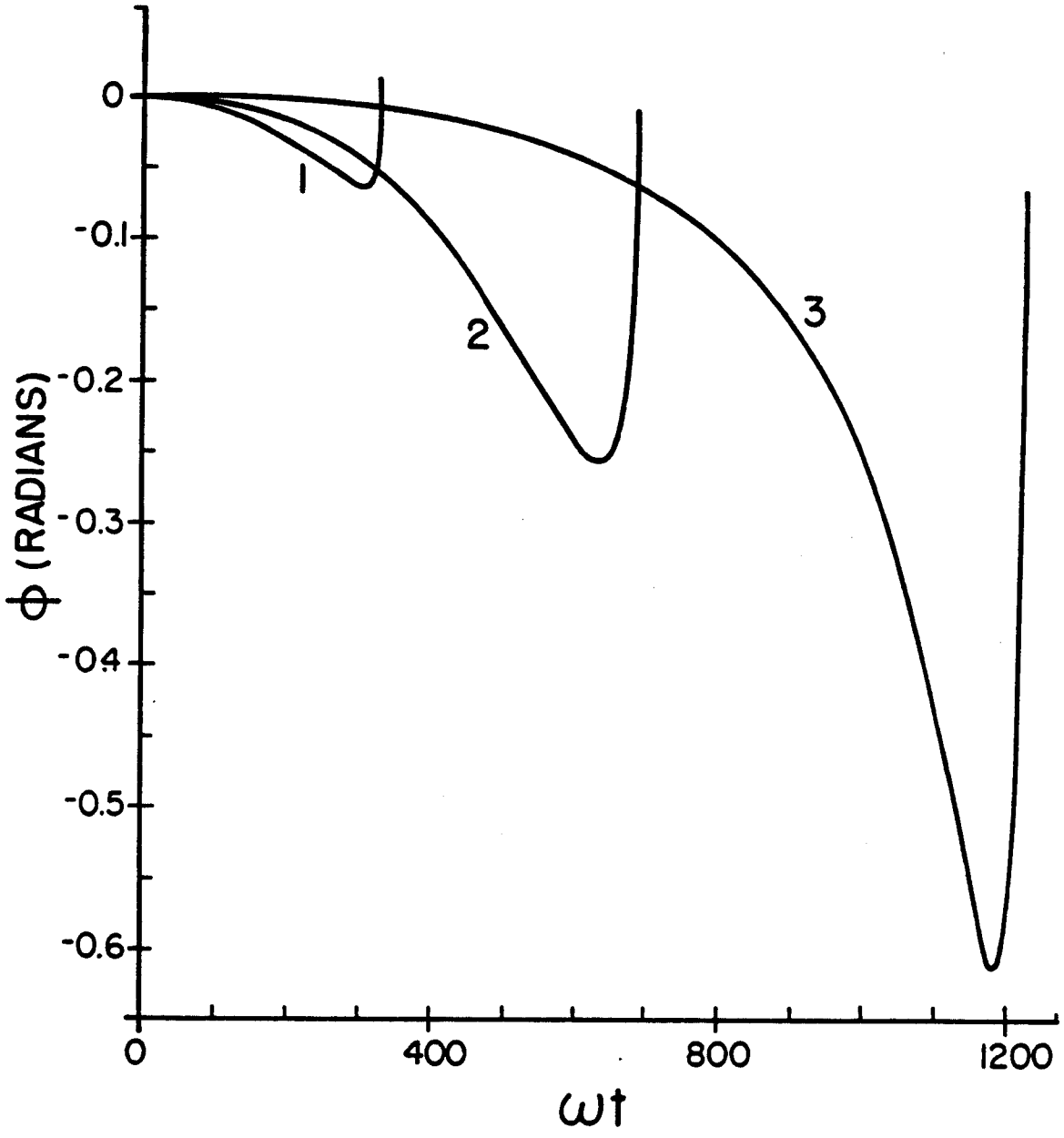

Figure 1b

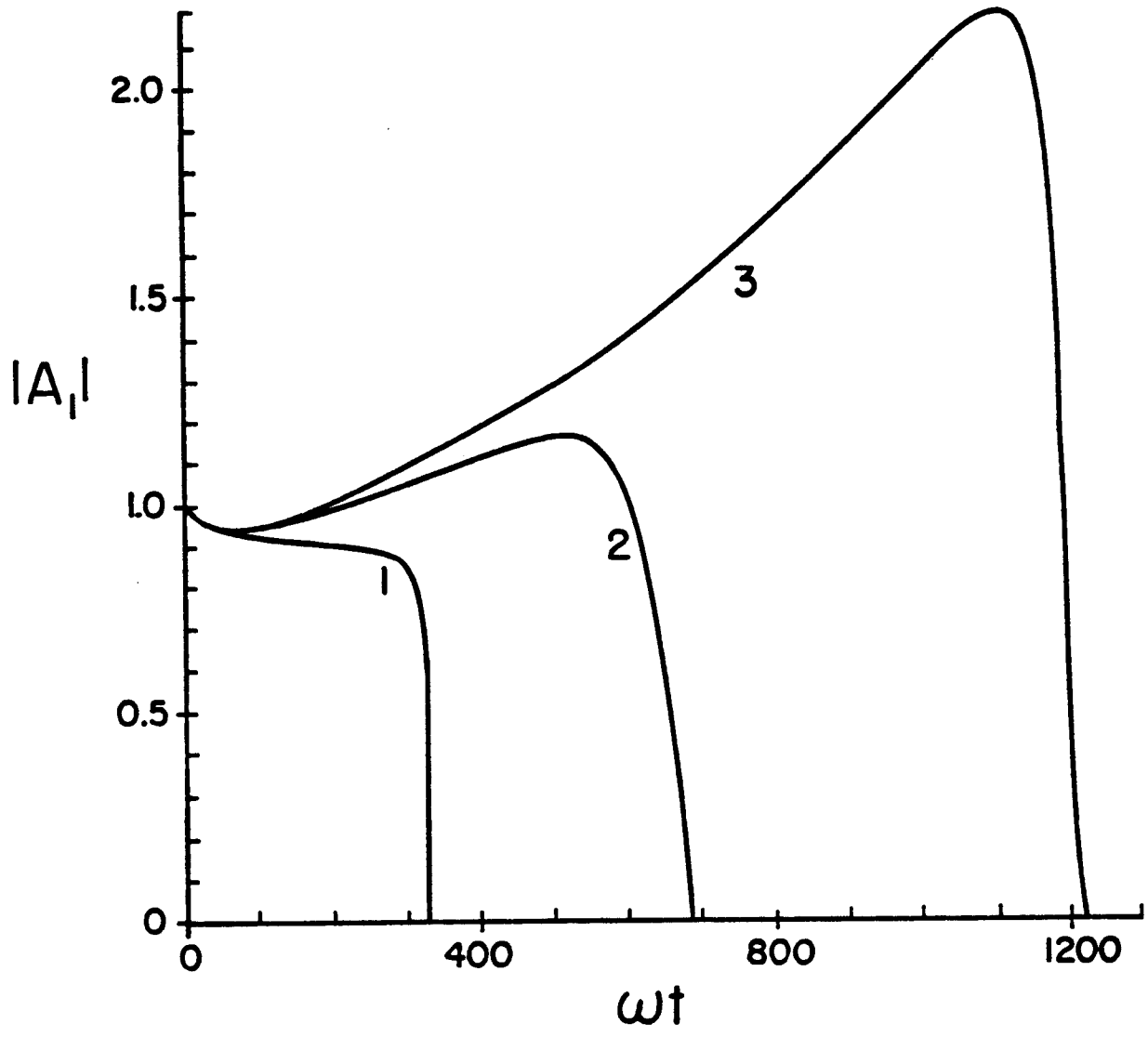

Figure 1c

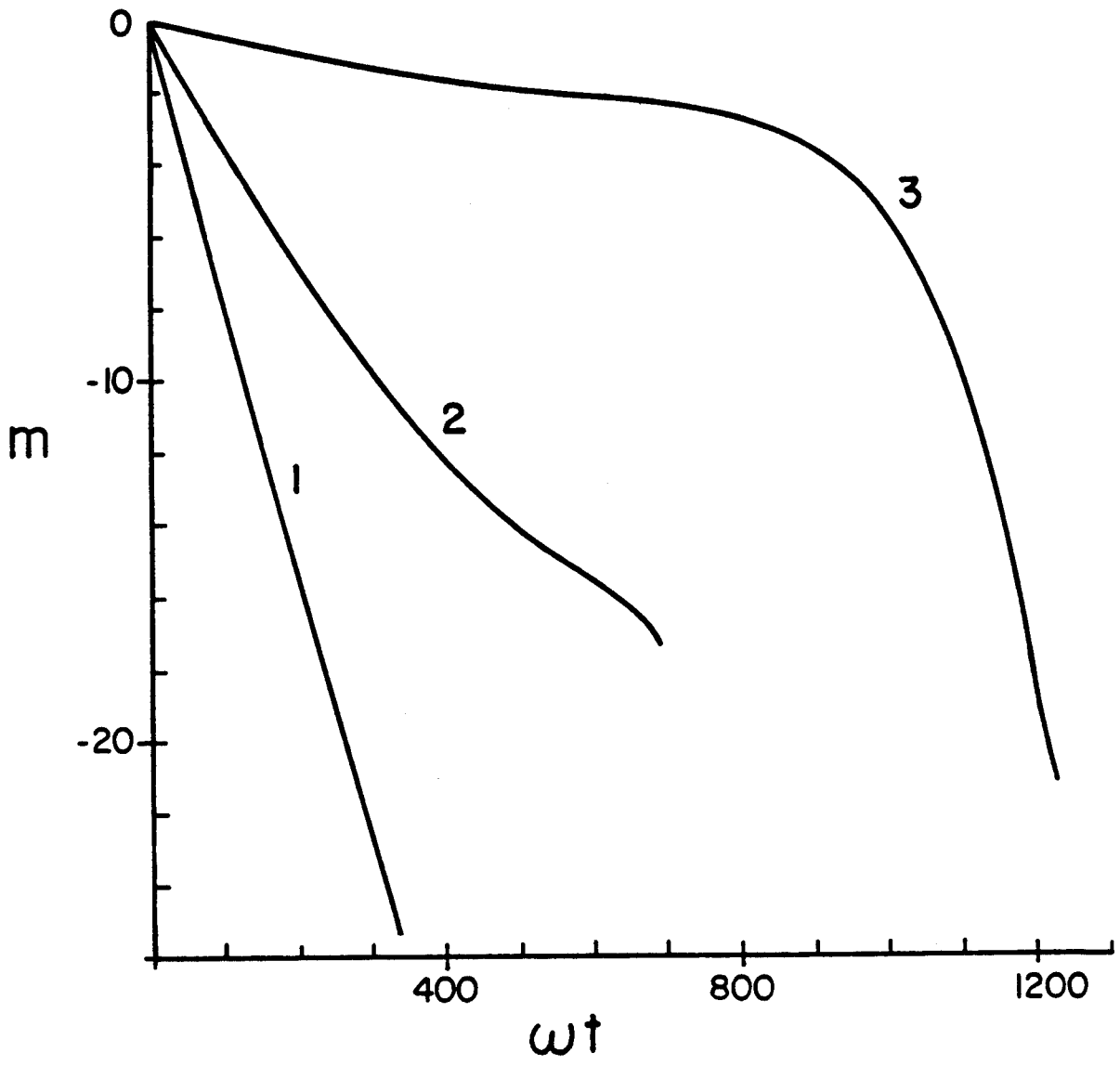

Figure 1d

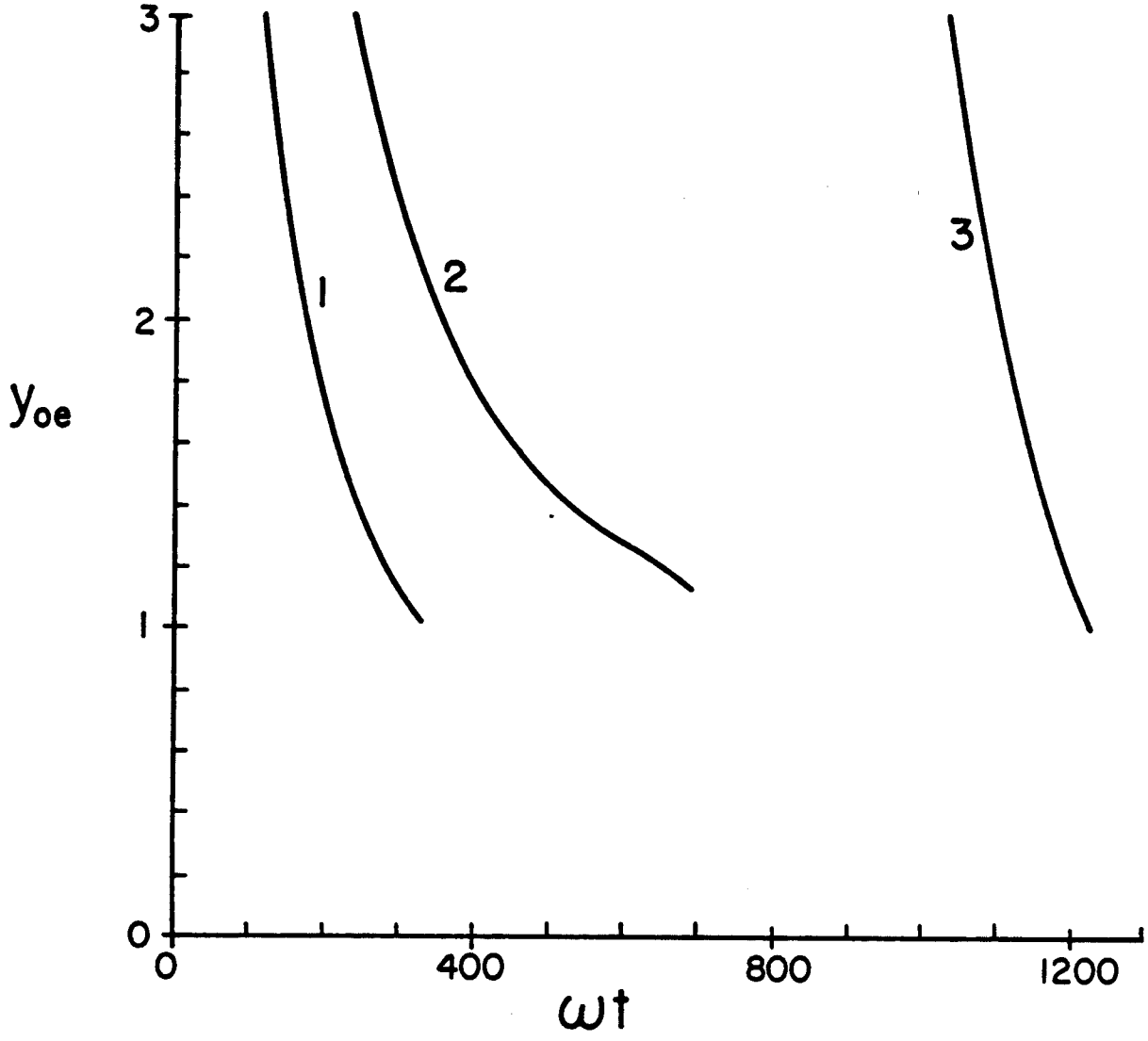

Figure 1e

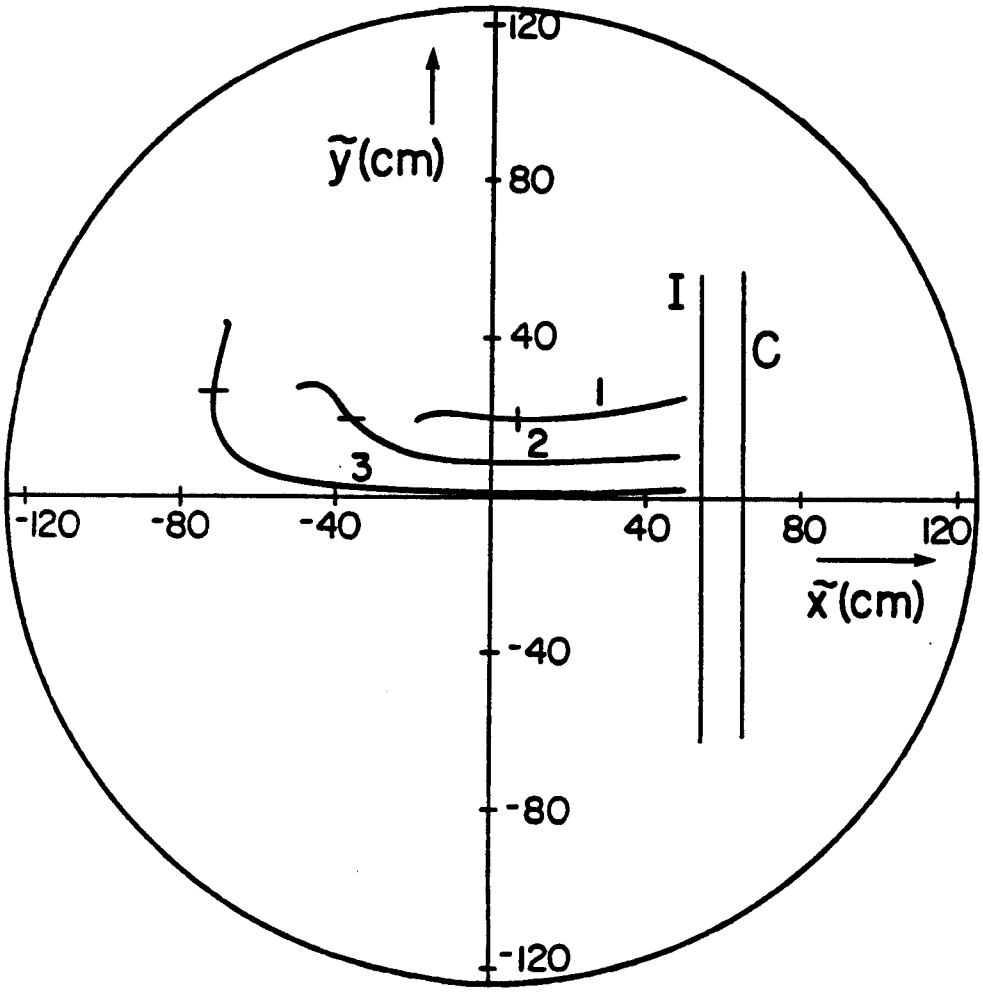

Figure 2

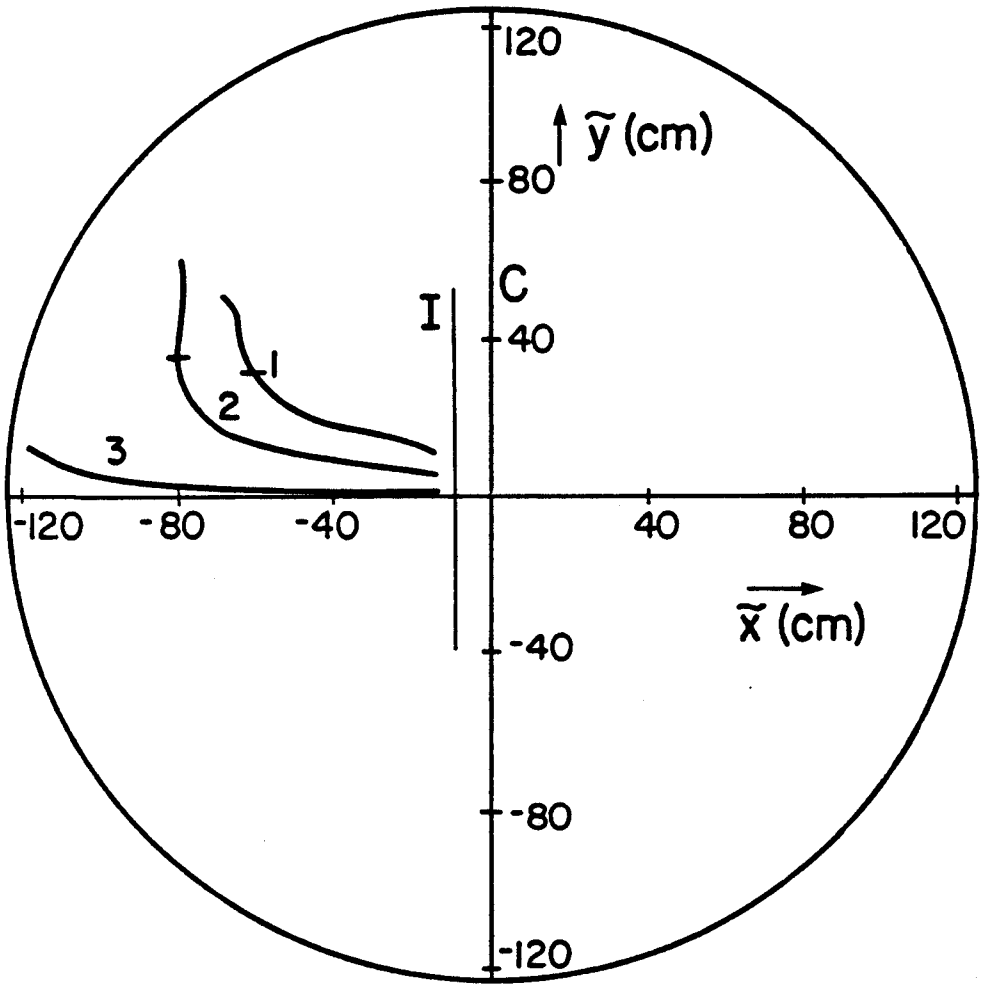

Figure 3a

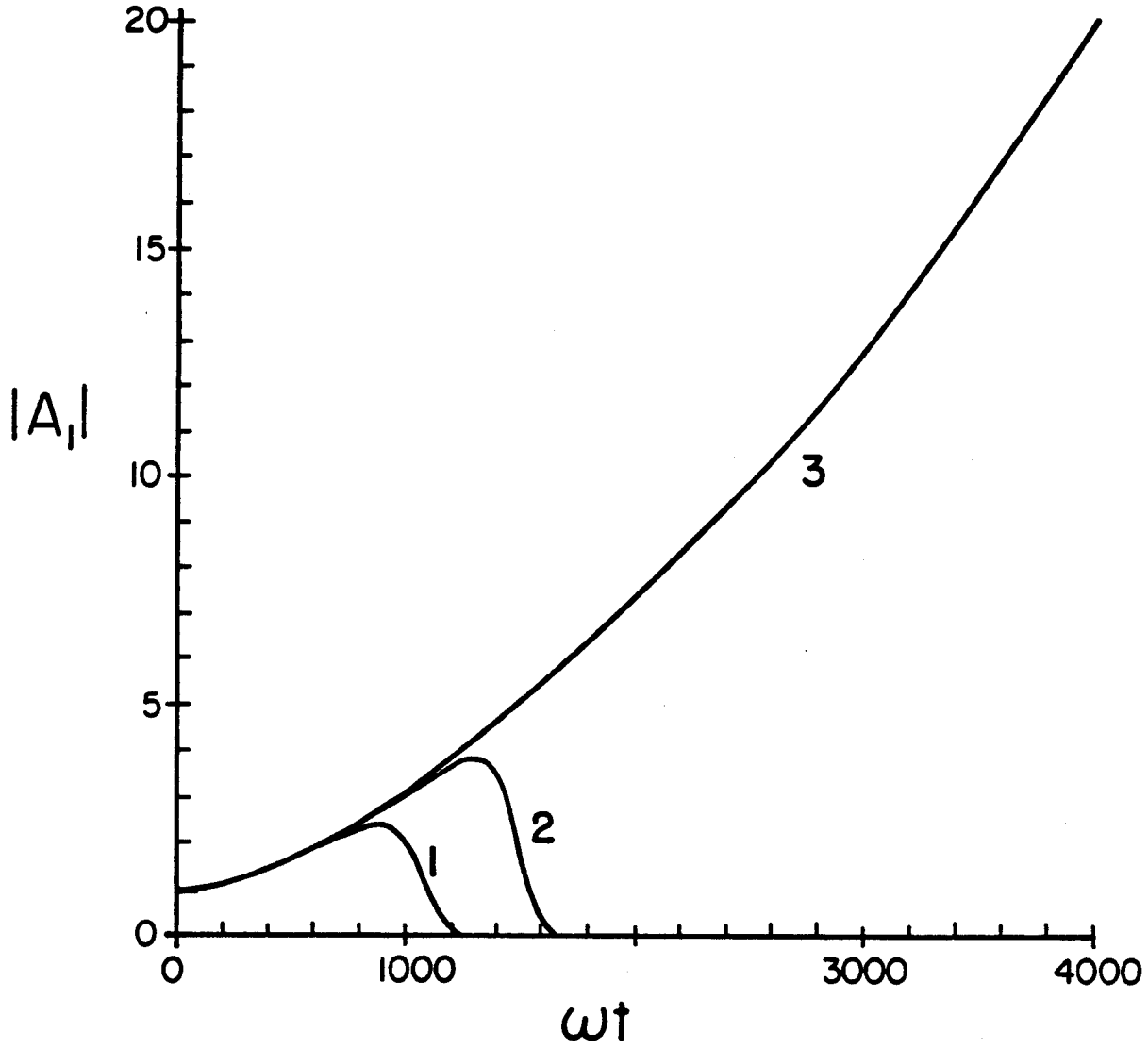

Figure 3b

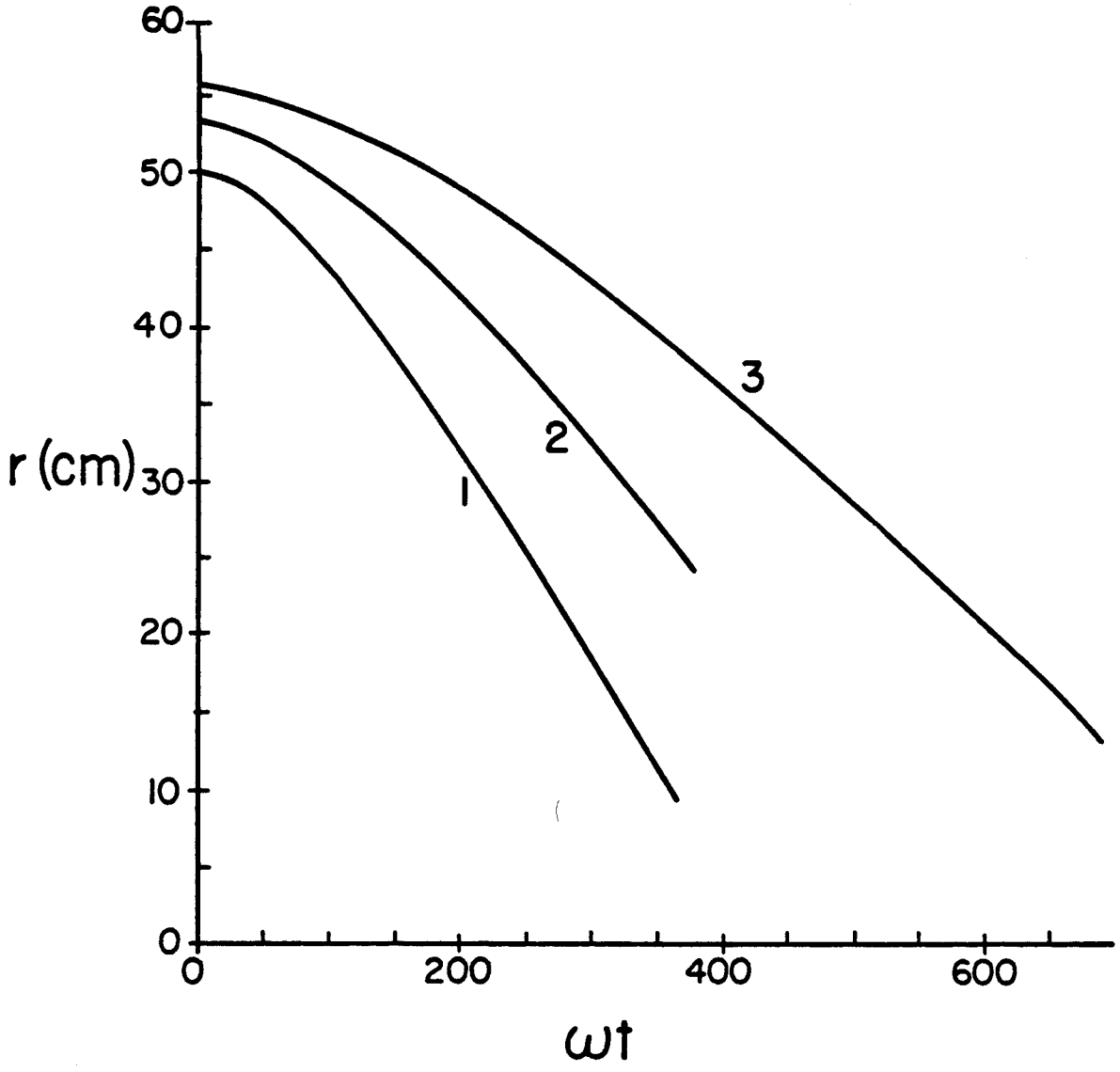

Figure 4

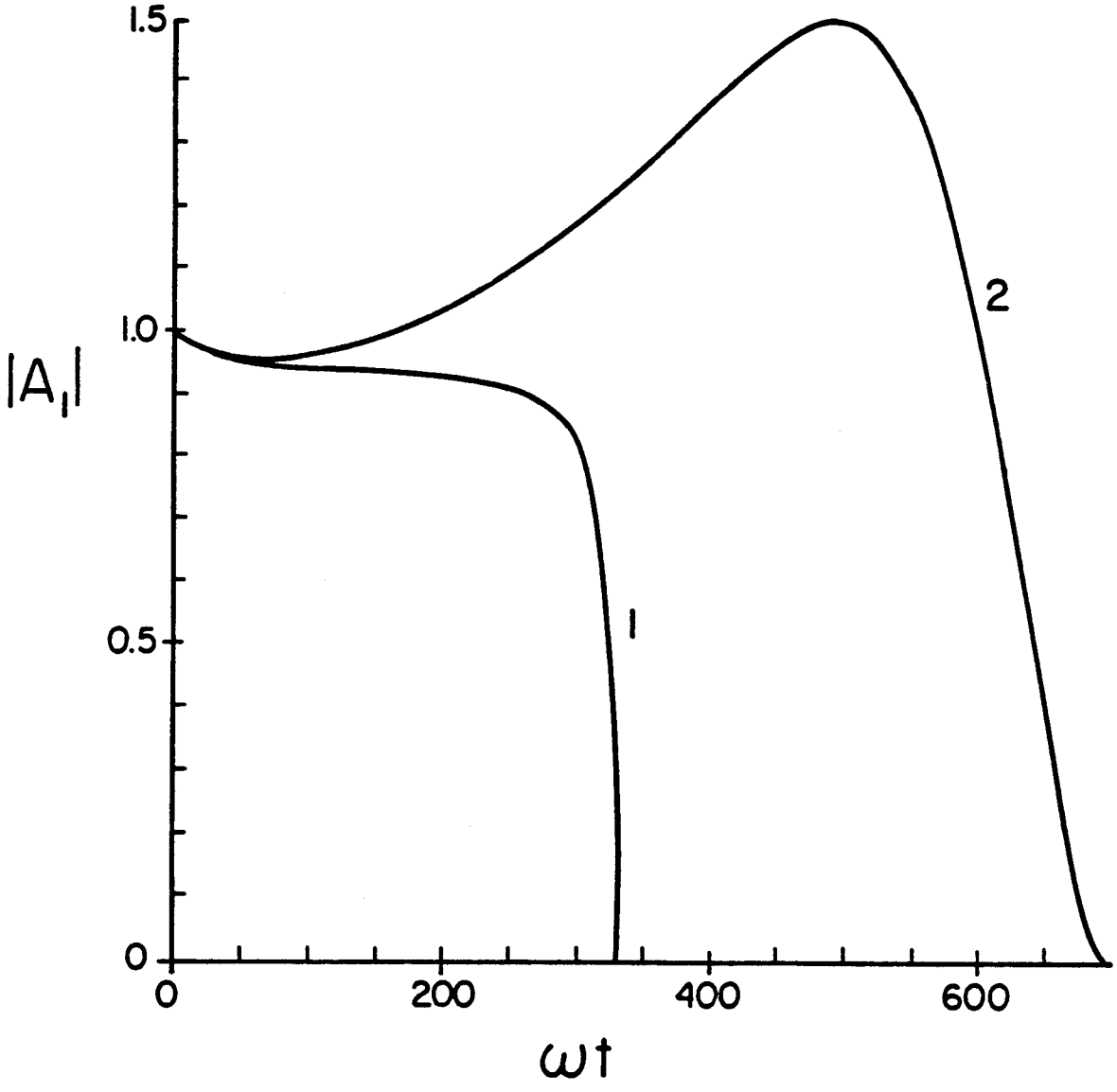

Figure 5

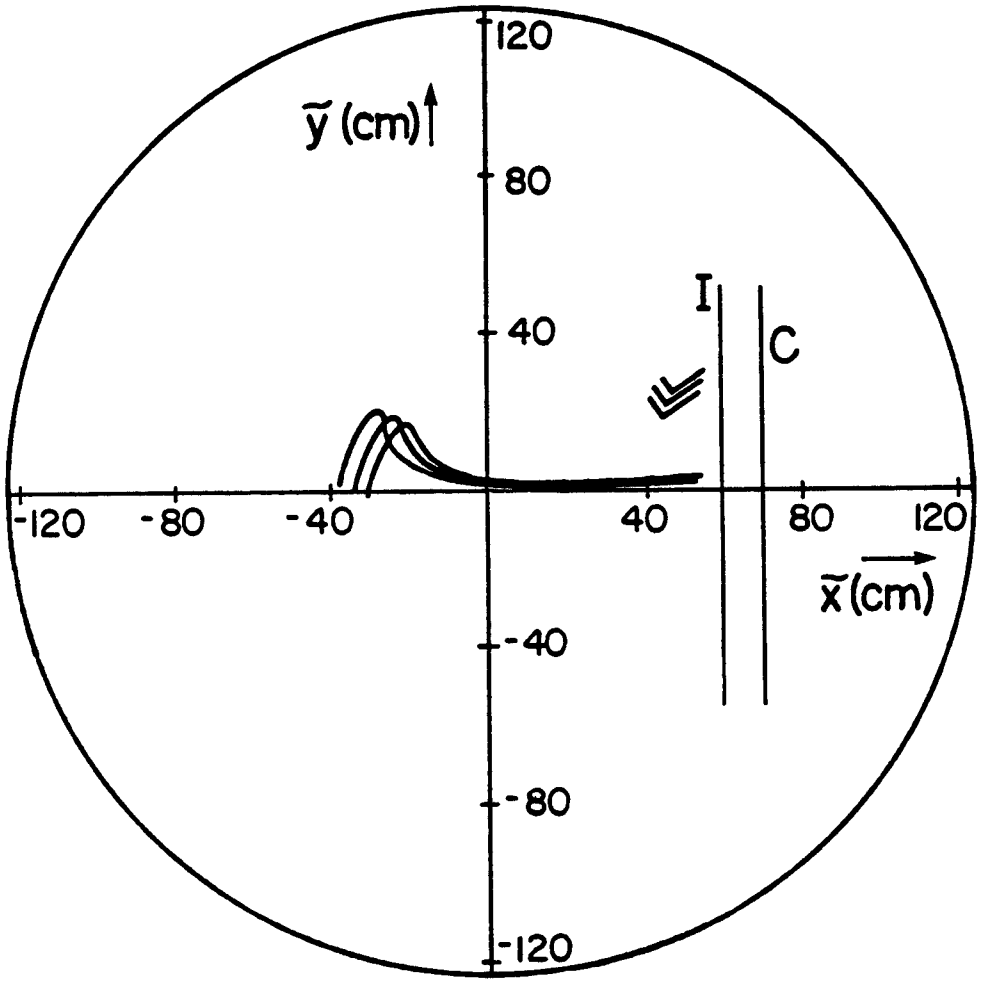

Figure 6